PHYSICS

Efficient nonreciprocal mode transitions in spatiotemporally modulated acoustic metamaterials

Zhaoxian Chen[1,2]†, Yugui Peng[3]†, Haoxiang Li[1]†, Jingjing Liu[1], Yujiang Ding[1], Bin Liang[1]*, Xue-Feng Zhu[4]*, Yanqing Lu[2], Jianchun Cheng[1]*, Andrea Alù[3,5]*

In linear, lossless, time-invariant, and nonbiased acoustic systems, mode transitions are time reversible, consistent with Lorentz reciprocity and implying a strict symmetry in space-time for sound manipulation. Here, we overcome this fundamental limitation by implementing spatiotemporally modulated acoustic metamaterials that support nonreciprocal sound steering. Our mechanism relies on the coupling between an ultrathin membrane and external biasing electromagnetic fields, realizing programmable dynamic control of the acoustic impedance over a motionless and noiseless platform. The fast and flexible impedance modulation of our metamaterial imparts an effective unidirectional momentum in space-time to realize nonreciprocal transitions in *k*-ω space between different diffraction modes. On the basis of these principles, we demonstrate efficient nonreciprocal sound steering, showcasing unidirectional evanescent wave conversion and nonreciprocal upconversion focusing. More generally, our metamaterial platform offers opportunities for generation of nonreciprocal Bloch waves and extension to other domains, such as non-Hermitian topological and parity-time symmetric acoustics.

INTRODUCTION

It is of fundamental interest and practical importance to mold the acoustic fields with the desired wavefront, but acoustic propagation in Hermitian systems obeying time reversal symmetry is always reversible under the constraint of Lorentz reciprocity (*1*). While magneto-optical phenomena are commonly used to break reciprocity in electromagnetics, magnetoacoustic phenomena are usually too weak to support efficient nonreciprocal sound propagation (*2*). Attempts to realize acoustic nonreciprocity trace back to the so-called acoustic diodes based on asymmetric nonlinearities (*3*–*5*), but they suffer from several drawbacks, including instabilities, distortion, limited efficiency, inherent dependence of the response on the excitation from multiple ports, and output phase chaos. The recent introduction of parity-time symmetry (*6*) in optics (*7*, *8*) and acoustics (*9*–*12*) has enabled anisotropic transmission resonances and unidirectional wave diffraction, which overcome constraints stemming from power conservation, but still obey reciprocity as long as the systems remain linear (*13*). In the past decade, progress in condensed matter physics has extended the paradigm of topological insulators from electronics (*14*) to photonics (*15*), mechanics (*16*), and acoustics (*17*). However, the bosonic nature of phonons makes the suppression of spurious reflections in the most common implementations of topological acoustic structures based on valley pseudo-spin very challenging because of the underlying reciprocity and unavoidable time-reversible mode coupling associated with disorders (*18*–*20*). Acoustic Chern insulators (*21*–*23*) or Floquet insulators (*24*–*26*) have offered opportunities to realize topologically robust one-way sound transport induced by broken reciprocity, but they have been relying on complex arrays of individually controlled piezoelectric elements, mechanically spinning elements, and/or vibrations controlled by motors (*27*, *28*). Nonreciprocal airborne sound steering remains elusive because of the challenges in the experimental realization of fast, efficient, and precisely tailored space-time modulation patterns that can enable irreversible mode transitions of choice in the frequency-momentum space.

Here, we overcome these limitations in terms of speed, efficiency, sensitivity, and precision of spatiotemporal modulation in acoustic metamaterials (*29*–*31*) and experimentally demonstrate a range of nonreciprocal mode transitions and steering for airborne sound waves. Avoiding slowly moving mechanical components (*32*, *33*), individually controlled piezoelectric elements in large arrays (*26*), or flows in bulky structures (*28*), our approach to spatiotemporally modulate the acoustic response of a metamaterial is based on thin resonating membranes coupled to an external electromagnetic field. As a convenient implementation, the metamaterial unit cell is designed using a thin film transducer driven by a programmable electronic circuit. We derive the required time variation of the spatial distribution of effective acoustic impedance to enable efficient nonreciprocal mode transitions and verify its functionality with numerical simulations and experimental measurements. Under the judiciously designed spatiotemporal modulation of the electroacoustic coupling strength, we show unidirectional acoustic mode transitions in the *k*-ω band diagram, breaking space-time reversal symmetry, as schematically shown in Fig. 1. This functionality enables nonreciprocal sound steering in various forms, including unidirectional evanescent wave conversion and nonreciprocal focusing of upconverted signals. Our study shows how spatiotemporally modulated metamaterials can produce totally new opportunities for the manipulation of sound in space-time.

RESULTS

Nonreciprocal acoustic mode transitions

Figure 1A schematically illustrates our acoustic metamaterial platform supporting ultrafast and efficient spatiotemporal modulation,

[1]Key Laboratory of Modern Acoustics, MOE, Institute of Acoustics, Department of Physics, Nanjing University, Nanjing 210093, People's Republic of China. [2]College of Engineering and Applied Sciences, Nanjing University, Nanjing 210093, People's Republic of China. [3]Photonics Initiative, Advanced Science Research Center, City University of New York, New York, NY 10031, USA. [4]School of Physics and Innovation Institute, Huazhong University of Science and Technology, Wuhan, Hubei 430074, People's Republic of China. [5]Physics Program, Graduate Center, City University of New York, New York, NY 10016, USA.
*Corresponding author. Email: aalu@gc.cuny.edu (A.A.); liangbin@nju.edu.cn (B.L.); xfzhu@hust.edu.cn (X.-F.Z.); jccheng@nju.edu.cn (J.C.)
†These authors contributed equally to this work.

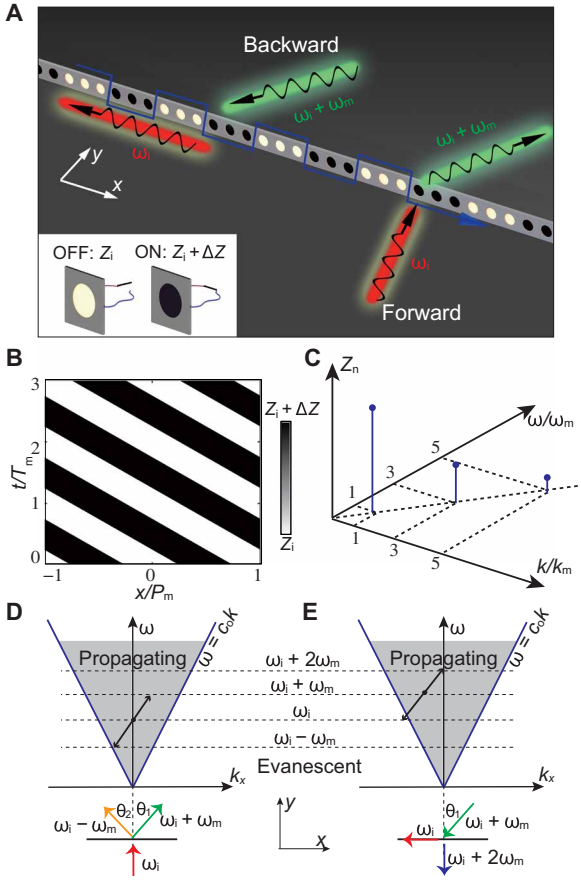

Fig. 1. Spatiotemporally modulated metamaterial array. (**A**) Schematic of nonreciprocal sound steering with space-time metamaterials. Inset: Two states of the unit cell comprising a membrane transducer and a programmable electronic circuit. The effective acoustic impedance of the unit changes from Z_i to $Z_i + \Delta Z$ when the circuit switches from "OFF" state to "ON" state. (**B**) Spatiotemporal modulation of impedance of the metamaterial array: By switching OFF and ON the relay in each element, the corresponding impedance is tuned between Z_i and $Z_i + \Delta Z$ with space and time periods P_m and T_m, respectively. (**C**) Fourier series expansion of the impedance in k-ω dimensions. (**D** and **E**) Nonreciprocal mode transition for waves traveling along (D) forward and (E) backward direction. The acoustic mode at ω_i and $k_x = 0$ is transformed into $\omega_i + \omega_m$ with $k_x = k_m$ and $\omega_i - \omega_m$ with $k_x = -k_m$, respectively. In the backward direction, the mode at $\omega_i + \omega_m$ and $k_x = -k_m$ is coupled back to ω_i, but outside the light cone.

enabling large nonreciprocity for sound steering. Each metamaterial unit cell is formed by a thin membrane, much smaller than the acoustic wavelength in all three dimensions, coupled to an external electromagnetic field with fast-varying and highly tunable strength. The capability of the membrane to interact with the incident acoustic wave depends on its coupling strength, enabling a fast and effective impedance modulation with no need for mechanical rotations or external air flow. For simplicity, and without loss of generality, in the current study, we implement this platform using a commercial membrane transducer, consisting of a deeply subwavelength thin film coupled to a coil controlled by a magnetic field, loaded by an auxiliary programmable circuit. In contrast to the conventional operation of a loudspeaker, which radiates sound through a vibrating film driven by the Lorentz force acting on the coil, here, the membrane transducer works as a passive acoustic component, and its coil, without any active electric signals fed in, serves as a load that can be controlled by an electric relay. When the relay switches ON, the acoustic impedance abruptly changes from Z_i to $Z_i + \Delta Z$, with Z_i and ΔZ being the intrinsic acoustic impedance of the thin film and the additional impedance resulting from the electroacoustic coupling, respectively. For a one-dimensional (1D) array of identical unit cells aligned along the x direction, as shown in Fig. 1A, a periodic modulation of the acoustic impedance can be implemented in space-time, with periods P_m and T_m, respectively, as shown in Fig. 1B, by programming the circuit to feed the relays with electric square wave signals with ordered phase sequences. Applying a Fourier expansion, the resulting surface impedance can be expressed as a series of sinusoidal components carrying different synthetic momenta

$$Z(x,t) = Z_0 + \sum_n Z_n \cos(n\omega_m t - nk_m x) \tag{1}$$

where the index n is an odd integer, $\omega = 2\pi/T_m$ is the modulating frequency, $k_m = 2\pi/P_m$ is the modulating spatial wave vector, Z_0 is the static acoustic impedance, and Z_n is the modulation strength of the nth-order sinusoidal component (see note S1 for a detailed derivation). We tailor the impedance modulation so that the first-order Fourier component dominates the response, as shown in Fig. 1C, because we want to enable a first-order frequency transition. When a plane wave mode with frequency ω_i and wave vector k_i impinges on the array, the transmitted wave will consist of blue-shifted and red-shifted Fourier components due to mixing over the surface with the modulation signal (*34*–*40*)

$$\begin{aligned} p(\mathbf{r},t) = {} & p_0 \exp(i\omega_i t - i\mathbf{k}_i \cdot \mathbf{r}) + \\ & p_1 \exp[i(\omega_i + \omega_m)t - i\mathbf{k}_i \cdot \mathbf{r} - ik_m x] + \\ & p_{-1} \exp[i(\omega_i - \omega_m)t - i\mathbf{k}_i \cdot \mathbf{r} + ik_m x] \end{aligned} \tag{2}$$

where p_0, p_1, and p_{-1} are the pressure amplitudes of the zeroth-, first-, and −first-order modes, and we neglect higher-order terms. Here, the synthetic linear momentum induced by the spatiotemporal modulation breaks reciprocity and it is expected to induce largely asymmetric mode transitions. For example, in Fig. 1D, an acoustic plane wave with frequency ω_i impinges normally ($k_x = 0$) on the spatiotemporally modulated array. The blue-shifted wave at $\omega_i + \omega_m$ acquires an additional momentum k_m in the x direction, emerging from the array at the refraction angle θ_1. However, in Fig. 1E, we study the time-reversed scenario of a wave with frequency $\omega_i + \omega_m$ propagating backwards from angle $-\theta_1$. The corresponding transmitted mode at frequency ω_i acquires additional momentum, exiting the light cone and turning into an evanescent wave. This is an indication of a largely nonreciprocal mode transition, which can be used to realize nonreciprocal excitation of evanescent waves.

Frequency conversion efficiency

Because of the deeply subwavelength nature of the unit cells in our array, the thin films vibrate like pistons, facilitating the modeling of the mode transitions in terms of time modulation (*41*). We can safely model the acoustic impedance as lumped parameters

$$Z_i = \left[\delta_m + i\left(M_m\omega - \frac{K_m}{\omega}\right)\right] \Big/ S_d \tag{3A}$$

$$\Delta Z = (BL)^2 / Z_e S_d \tag{3B}$$

where δ_m, M_m, and K_m are the mechanical damping coefficient, mass, and stiffness of the thin film, respectively; $S_d = \pi d^2/4$ is the radiation area determined by the diameter d; Z_e is its electric impedance; and the force factor BL enables ultrafast modulation of the electroacoustic coupling strength. All these parameters can be measured or calculated using the model from Klippel (*42*) as described in Materials and Methods. In our experiments, as schematically shown in Fig. 2 (A and B), the sample has a diameter d = 2 cm, which is integrated in a 3D printed holder and fixed to the impedance tube with an inner diameter of 5 cm. The relay in the transducer circuit is controlled by a single-chip microcomputer (SCM), which can modulate the transducer impedance at will in each element. The sample has a resonance frequency of around 970 Hz, with acoustic impedance predicted by Eqs. 3A and 3B of $Z_i = 95\ \mathrm{N \cdot s/m^3}$ and $Z_i + \Delta Z = 131\ \mathrm{N \cdot s/m^3}$, respectively, for the relay in the OFF and ON position. The transmission and reflection spectra were simulated by COMSOL Multiphysics: At 970 Hz, as shown in Fig. 2C, the transmission peak decreases from 0.53 to 0.45, while the reflection increases from 0.47 to 0.55 after the relay switches on. The peak frequency is not notably affected because of the small inductance of the sample. We also experimentally measured transmission and reflection based on the four-microphone method (*43*), as shown in Fig. 2D, with results in fairly good agreement with simulations. The small deviation observable between simulations and measurements may result from the simplified lumped parameter circuit used in our simulations to model the transducers. These results verify that the metamaterial unit cell impedance can be effectively modulated by the driving circuit.

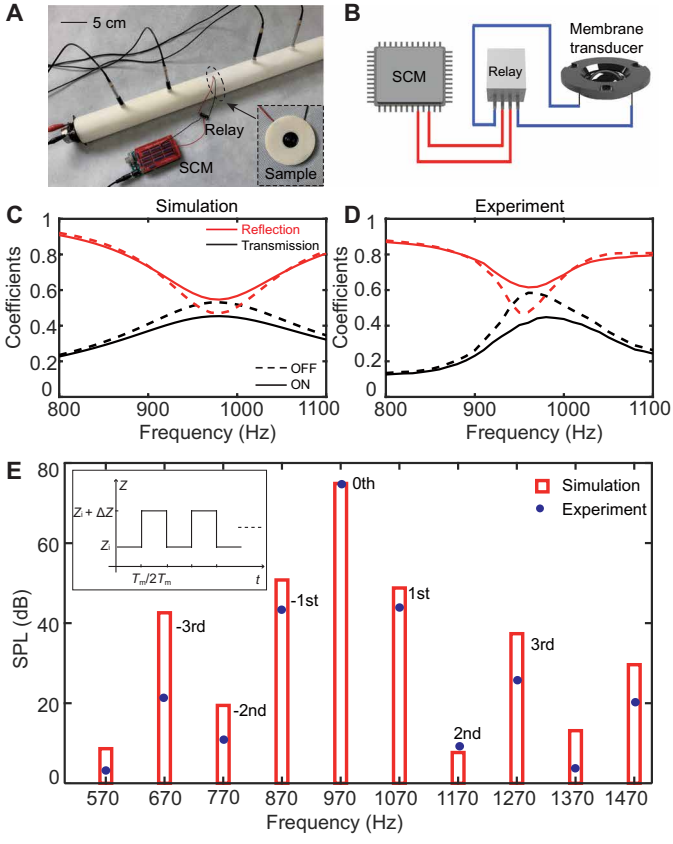

Fig. 2. Space-time mode transitions. (**A**) Acoustic setup to measure the mode transitions and extract the acoustic properties of the designed time-modulated metamaterial unit cell. The diameter of the impedance tube is 5 cm. A loudspeaker is fixed at one end, and absorptive foam is placed at the other end to eliminate reflections. Four microphones are used to extract the pressure amplitude and phase information. The membrane transducer connects to a relay, which is controlled by the SCM. The inset gives a clear view of the fabricated sample of a metamaterial unit cell, where the transducer has a diameter of 2 cm and it is positioned by a 3D printed holder. (**B**) Working principle of the electrically controlled impedance modulation. The outer two feet of the relay connect to the transducer's electrodes, while the inner two feet connect to the SCM. (**C**) Simulated and (**D**) measured transmission and reflection coefficients of the sample with the relay switching on and off. (**E**) Simulated and measured transmitted sound pressure level (SPL) at the operation frequency and blue/red-shift frequencies. Here, the operation frequency is 970 Hz, and the sample is modulated at 100 Hz by a square voltage wave. Photo credit: Zhaoxian Chen, Nanjing University.

To demonstrate an efficient nonreciprocal mode transition in space-time, the sound frequency was set at 970 Hz, with relays modulated by an electric square wave signal at 100 Hz. As shown in Fig. 2E, the measured transmission spectrum presents a series of blue-shifted and red-shifted peaks spaced by multiples of the modulation frequency. With a square wave modulation, shown in the inset, the odd-order modes are stronger than the even-order ones (see more details in note S2). The finite-difference time-domain simulations agree well with the experimental measurements. However, because of unavoidable relaxation effects in the electroacoustic coupling, there is a trade-off between the modulation frequency and the frequency conversion efficiency, and the measured sound pressure levels (SPLs) are slightly lower than the simulation results. Specifically, according to the experimental results, the power efficiency for the first-order harmonic conversion is 1.5×10^{-4}, which is independent of the incident power and could be further improved by enhancing the modulation strength (see note S3 for detailed calculations, discussions, and simulations about power efficiency). Without other resonating structures, viscothermal loss here is quite small and has a negligible effect on the mode transitions (see note S4 for the demonstration). In addition, from the viewpoint of power efficiency, the operational bandwidth of the mode transition in our system is about 250 Hz (see note S5 for more discussions).

Unidirectional evanescent wave conversion

Next, we apply our space-time acoustic metamaterial to demonstrate nonreciprocal wave-steering functionalities. The array is aligned in the x direction, with an initial phase of impedance modulation implementing a uniform gradient $d\varphi/dx$ distribution, as shown in Fig. 3A, which implements a constant spatial gradient of impedance over the surface. The spatiotemporal modulation of the impedance imparts a traveling wave, with modulation frequency ω_m, which transforms the spatial gradient into a synthetic linear momentum bias breaking reciprocity. On the basis of momentum conservation, the generalized Snell's law for the first-order blue-shifted mode follows

$$k_i \sin(\theta_i) + d\varphi/dx = k_1 \sin(\theta_1) \quad (4)$$

where k_i and θ_i are the wave vector and incident angle of the incident waves at frequency ω_i, and k_1 and θ_1 are the wave vector and refraction angle of the output wave at $\omega_i + \omega_m$. The relation between θ_i and θ_1 is shown by the green curve in Fig. 3B, where $\omega_i/2\pi$ = 1000 Hz, $\omega_m/2\pi$ = 1000 Hz, and $d\varphi/dx = 2\pi/60\ \mathrm{cm^{-1}}$. As we time-reverse the outgoing wave, becoming an incident wave at $\omega_i/2\pi$ = 1100 Hz,

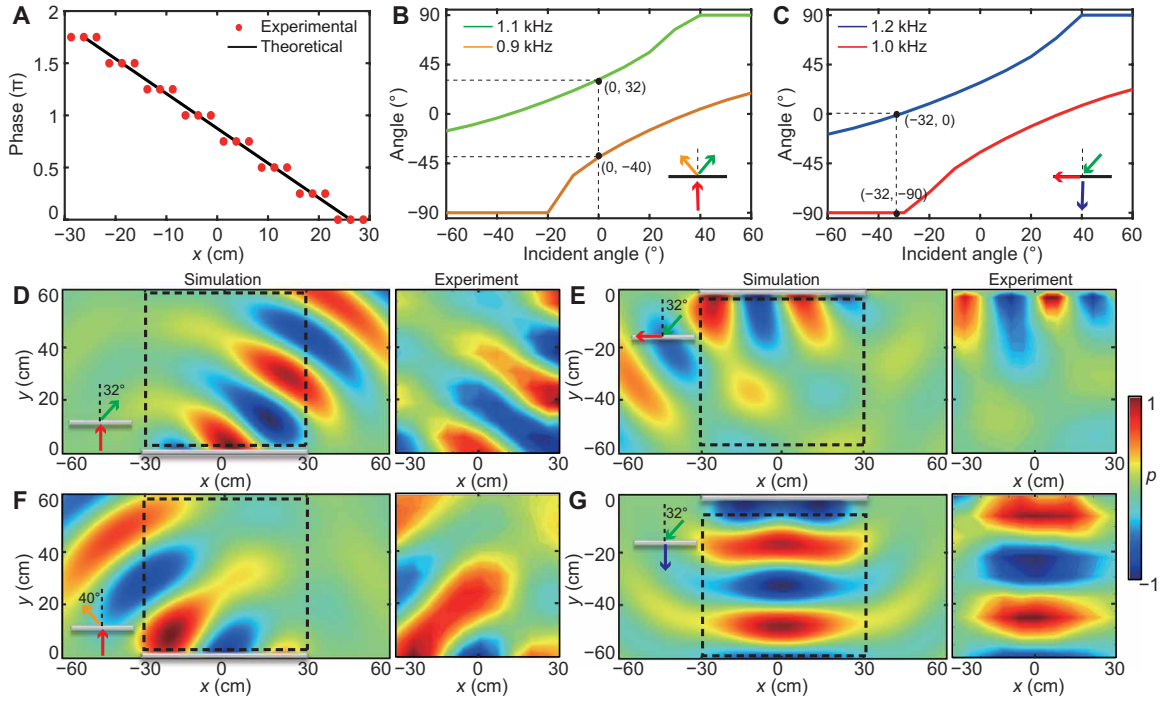

Fig. 3. Nonreciprocal evanescent wave conversion. (**A**) Initial phase distribution of the impedance modulation to generate unidirectional evanescent wave conversion. The metamaterial consists of 24 time-varying unit cells, for a total length of 60 cm. The adjacent three unit cells are set as a subgroup, and the phase lag is π/4. (**B**) Refraction angles for outgoing acoustic waves at 1100 Hz (green curve) and 900 Hz (yellow curve) with a forward incidence of 1000 Hz. (**C**) Refraction angles for outgoing acoustic waves at 1200 Hz (blue curve) and 1000 Hz (red curve) for a backward incidence of 1100 Hz. (**D** to **G**) Simulated and measured pressure field distributions for a nonreciprocal mode transition, corresponding to the four cases marked by the black dots in (B) and (C). The dashed boxes mark the measurement areas.

the mode is red-shifted back to the original frequency $(\omega_i - \omega_m)/2\pi$ = 1000 Hz, but now obeying the relation

$$k_i \sin(\theta_i) - d\varphi/dx = k_{-1} \sin(\theta_{-1}) \quad (5)$$

where k_{-1} and θ_{-1} are the wave vector and refraction angle of the −first-order mode. The relation between θ_i and θ_{-1} is shown by the red curve in Fig. 3C, with the −first-order mode at 900 Hz shown as the yellow curve in Fig. 3B and the first-order mode at 1200 Hz shown as the blue curve in Fig. 3C. From Fig. 3 (B and C), we clearly see that a nonreciprocal mode transition is expected for a wide range of incidence angles, $\theta_i = -1° \sim 32°$. For example, as marked by the black dots in Fig. 3 (B and C), for the forward propagating signal at $\theta_i = 0°$ and $\omega_i/2\pi$ = 1000 Hz, the refraction angle and frequency of the blue-shifted outgoing mode are $\theta_1 = 32°$ and $(\omega_i + \omega_m)/2\pi$ = 1100 Hz. By reversing the outgoing signal into a backward incoming wave at $\theta_i = -32°$ and $\omega_i/2\pi$ = 1100 Hz, the red-shifted transmitted wave will emerge at $\theta_{-1} = -90°$ and $(\omega_i - \omega_m)/2\pi$ = 1000 Hz, which is an evanescent mode traveling along the metamaterial surface, instead of leaving the surface in the normal direction, largely breaking reciprocity. We note that the nonreciprocal response can be maintained over a quite broad frequency range (see more details in note S5). In experiments, the impinging plane waves are generated by eight loudspeakers equally spaced by 10 cm, and the spatiotemporal metamaterial is placed 30 cm away from the line source (more details in note S6). The measured results agree well with simulations, as shown in Fig. 3 (D and E), and clearly display unidirectional evanescent wave coupling (*44*), largely breaking reciprocity. To provide a full view of the mode transition process, Fig. 3 (F and G) shows the −first-order mode at 900 Hz for forward propagation and the first-order mode at 1200 Hz for backward propagation, respectively. This nonreciprocal response allows efficient radiation of acoustic energy toward the target direction, while avoiding reflections traveling back toward the source. Instead, they are trapped as surface waves, opening the possibility for the design of novel functional devices, such as nonreciprocal phased arrays with applications in noninvasive acoustic imaging and communications.

Nonreciprocal focusing of upconverted waves

Last, we reconfigure the space-time metamaterial to enable the functionality of a nonreciprocal acoustic metalens. For a plane wave at 1000 Hz normally impinging on the metamaterial, we design the initial phase distribution of impedance modulation to focus the upconverted first-order mode at 1100 Hz to a prescribed focal point. The spatial distribution of the modulation phases follows (*45*)

$$\varphi(x) = k_1(\sqrt{x^2 + y^2} - y) \quad (6)$$

where the focal point is located at y = 30 cm and the phase distribution is shown in Fig. 4A. In our experiments, the phase lag between adjacent unit cells is π/8. The phase profile is again spatiotemporally modulated to create focusing for the upconverted signal, as verified in simulations and experiments shown in Fig. 4B, in good agreement with each other. To quantitatively investigate the focusing effect, we plot the normalized intensity distribution along the actual focal plane at y = 25 cm, shown in Fig. 4C. The full width at half maximum of the blue-shifted focal spot is around 16 cm, less than half the wavelength of sound at 1000 Hz (more details in notes

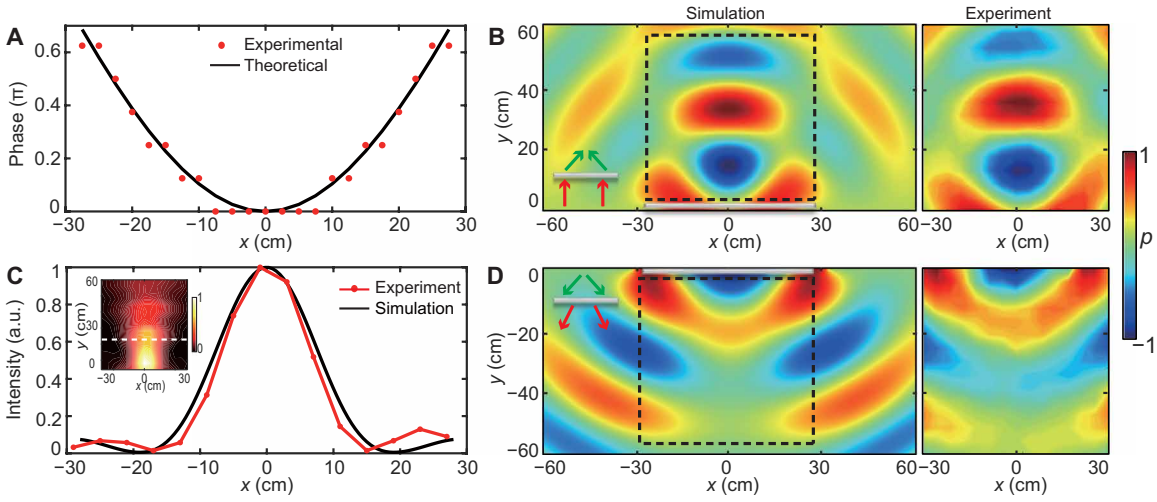

Fig. 4. Nonreciprocal focusing of upconverted waves. (**A**) Initial phase distribution of the impedance modulation to generate nonreciprocal blue-shift focusing. The focus is designed at $y = 30$ cm behind the metamaterial, and the phase lag in the sample is $\pi/8$. (**B**) Simulated and measured focusing fields at 1100 Hz for normal incidence at 1000 Hz. (**C**) Sound intensity distribution along the cut line at $y = 25$ cm in (B), which is the focal position. The inset plots the normalized intensity field. (**D**) Simulated and measured diverging fields at 1000 Hz for reversed incidence in the backward direction at 1100 Hz, with a point source placed at $x = 0$ cm and $y = 25$ cm. a.u., arbitrary units.

Table 1. Average small signal parameters of the transducers.

Parameter	Notation	Value	Unit
DC resistance	R_e	8.5	Ohm
Coil inductance	L_e	0.03	mH
Force factor	BL	0.3	N/A
Moving mass	M_m	0.05	g
Mechanical resistance	δ_m	0.027	kg/s
Mechanical stiffness	K_m	1.86	N/mm
Resonating frequency	f_0	970	Hz

S7 and S8), hence breaking the diffraction limit, thanks to the upconversion phenomenon that shrinks the wavelength. The focal plane is slightly closer to the sample surface than the designed one because of the discretization of the phase distribution. For a conventional metalens with a static phase gradient, the focusing effect obeys reciprocity and time reversal symmetry. Here, on the contrary, if we put a point source with frequency 1100 Hz at the focal point $x = 0$ cm and $y = 25$ cm, the red-shifted mode at 1000 Hz forms a divergent beam instead of a collimated one, as shown in Fig. 4D, indicating that sound focusing is strongly nonreciprocal (*46*). Such a response has far-reaching implications in important scenarios ranging from ultrasound therapy to nondestructive evaluation, which calls for high-efficiency conversion of acoustic energy but traditionally suffers from undesired reversed wave propagation back to the source.

DISCUSSION

Here, we have demonstrated the emergence of nonreciprocal mode transitions in a highly efficient, reconfigurable spatiotemporal acoustic metamaterial. By carefully tailoring the spatiotemporal modulation profile of a metamaterial array, we imparted synthetic momentum bias in various forms to realize efficient nonreciprocal mode transitions of choice in k-ω space. We have successfully demonstrated unidirectional evanescent wave conversion and nonreciprocal upconverted wave focusing, which would be impossible in time-invariant, static acoustic systems. Although piezoelectric patches have been successfully used for designing elastic wave modulation systems (*26*), they are characterized by large resistances and are not applicable for airborne sound. Besides, their modulation efficiency is limited, and the system robustness is hindered because active components are required in the electric circuit, leading to potential instabilities. Compared with other time-varying modulation schemes, such as mechanical vibrations or flow circulation, our electrically controlled switched membranes feature various advantages to implement giant and tailorable nonreciprocal transitions. First of all, the modulation frequency can be extended up to 1000 Hz owing to the fast relay response. In addition, without the additional noise originating from vibrating or rotating components, the proposed system is notably more robust. Nonetheless, the transition efficiency in this work can be further improved by increasing the force factor BL or introducing resonant metastructures. By tailoring the spatiotemporal modulation along the waveguide structures, our mechanism can be further extended to implement various nonreciprocal acoustic functionalities, such as gyrators and circulators (*47*, *48*). Our proposal can be flexibly merged with 3D acoustic time-varying metamaterials, opening unique opportunities to explore nonreciprocal topological acoustics, and acoustic physics in synthetic dimensions.

MATERIALS AND METHODS

Experiments

We use commercial coil-moving electroacoustic membrane transducers as the unit cells of our metamaterial, with linear parameters, as shown in Table 1, measured by the small signal Klippel system.

The relays of SIP-1A05 are used as switches to control the impedance of the metamaterial. In the impedance tube experiment (Fig. 2), four 1/4-inch-diameter microphones (Brüel and Kjaer Type 4961) and a multichannel analyzer (Brüel and Kjaer Pulse Type 3160) are used to extract the pressure information. In the 2D sound field steering experiment, a single-chip computer (Arduino Mega 2560) is used to provide multichannel square wave voltage signals with elaborately programmed frequency and phase lag for controlling the relays. The measurement is performed in a 2D parallel waveguide made of acrylic boards (more details in note S6).

Numerical simulations

A commercial finite element method (FEM) software (COMSOL Multiphysics) is used for the numerical study. For obtaining the simulated transmission and reflection in Fig. 2 (C and D), the acoustic module and frequency domain solver are used with the ultrathin transducer treated as an impedance boundary calculated according to Eqs. 3A and 3B. The mass density and sound speed of air are set as $\rho_0 = 1.21\ kg/m^3$ and $c_0 = 343\ m/s$, respectively. For the transmitting SPL analysis, we first use the transient solver and physics module to get the transmitting pressure information and then fast Fourier transformation to calculate its spectrum. All the simulated spatial distributions of acoustic field in both this paper and the Supplementary Notes are also obtained by using the frequency domain solver.

SUPPLEMENTARY MATERIALS

Supplementary material for this article is available at https://science.org/doi/10.1126/sciadv.abj1198

REFERENCES AND NOTES

1. H. Nassar, B. Yousefzadeh, R. Fleury, M. Ruzzene, A. Alù, C. Daraio, A. N. Norris, G. Huang, M. R. Haberman, Nonreciprocity in acoustic and elastic materials. *Nat. Rev. Mater.* **5**, 667–685 (2020).
2. A. Yariv, P. Yeh, *Optical Waves in Crystal Propagation and Control of Laser Radiation* (Wiley, 1983).
3. B. Liang, B. Yuan, J. C. Cheng, Acoustic diode: Rectification of acoustic energy flux in one-dimensional systems. *Phys. Rev. Lett.* **103**, 104301 (2009).
4. B. Liang, X. S. Guo, J. Tu, D. Zhang, J. C. Cheng, An acoustic rectifier. *Nat. Mater.* **9**, 989–992 (2010).
5. N. Boechler, G. Theocharis, C. Daraio, Bifurcation-based acoustic switching and rectification. *Nat. Mater.* **10**, 665–668 (2011).
6. C. M. Bender, S. Boettcher, Real spectra in non-hermitian hamiltonians having PT symmetry. *Phys. Rev. Lett.* **80**, 5243–5246 (1998).
7. H. Zhao, L. Feng, Parity–time symmetric photonics. *Natl. Sci. Rev.* **5**, 183–199 (2018).
8. M.-A. Miri, A. Alù, Exceptional points in optics and photonics. *Science* **363**, eaar7709 (2019).
9. X. Zhu, H. Ramezani, C. Shi, J. Zhu, X. Zhang, PT-symmetric acoustics. *Phys. Rev. X* **4**, 031042–031047 (2014).
10. T. Liu, X. Zhu, F. Chen, S. Liang, J. Zhu, Unidirectional wave vector manipulation in two-dimensional space with an all passive acoustic parity-time-symmetric metamaterials crystal. *Phys. Rev. Lett.* **120**, 124502 (2018).
11. R. Fleury, D. L. Sounas, A. Alù, Negative refraction and planar focusing based on parity-time symmetric metasurfaces. *Phys. Rev. Lett.* **113**, 023903 (2014).
12. R. Fleury, D. Sounas, A. Alù, An invisible acoustic sensor based on parity-time symmetry. *Nat. Commun.* **6**, 5905 (2015).
13. L. Feng, Y. L. Xu, W. S. Fegadolli, M. H. Lu, J. E. B. Oliveira, V. R. Almeida, Y. F. Chen, A. Scherer, Experimental demonstration of a unidirectional reflectionless parity-time metamaterial at optical frequencies. *Nat. Mater.* **12**, 108–113 (2013).
14. X.-L. Qi, S.-C. Zhang, Topological insulators and superconductors. *Rev. Mod. Phys.* **83**, 1057–1110 (2011).
15. L. Lu, J. D. Joannopoulos, M. Soljačić, Topological photonics. *Nat. Photonics* **8**, 821–829 (2014).
16. J. Cha, K. W. Kim, C. Daraio, Experimental realization of on-chip topological nanoelectromechanical metamaterials. *Nature* **564**, 229–233 (2018).
17. G. Ma, M. Xiao, C. T. Chan, Topological phases in acoustic and mechanical systems. *Nat. Rev. Phys.* **1**, 281–294 (2019).
18. Y. G. Peng, C. Z. Qin, D. G. Zhao, Y. X. Shen, X. Y. Xu, M. Bao, H. Jia, X. F. Zhu, Experimental demonstration of anomalous Floquet topological insulator for sound. *Nat. Commun.* **7**, 13368 (2016).
19. C. He, X. Ni, H. Ge, X. C. Sun, Y. B. Chen, M. H. Lu, X. P. Liu, Y. F. Chen, Acoustic topological insulator and robust one-way sound transport. *Nat. Phys.* **12**, 1124–1129 (2016).
20. J. Lu, C. Qiu, L. Ye, X. Fan, M. Ke, F. Zhang, Z. Liu, Observation of topological valley transport of sound in sonic crystals. *Nat. Phys.* **13**, 369–374 (2017).
21. Z. Yang, F. Gao, X. Shi, X. Lin, Z. Gao, Y. Chong, B. Zhang, Topological acoustics. *Phys. Rev. Lett.* **114**, 114301 (2015).
22. X. Ni, C. He, X. C. Sun, X. P. Liu, M. H. Lu, L. Feng, Y. F. Chen, Topologically protected one-way edge mode in networks of acoustic resonators with circulating air flow. *New J. Phys.* **17**, 053016 (2015).
23. A. B. Khanikaev, R. Fleury, S. H. Mousavi, A. Alu, Topologically robust sound propagation in an angular-momentum-biased graphene-like resonator lattice. *Nat. Commun.* **6**, 8260 (2015).
24. R. Fleury, A. B. Khanikaev, A. Alu, Floquet topological insulators for sound. *Nat. Commun.* **7**, 11744 (2016).
25. Y.-G. Peng, Y. Li, Y. X. Shen, Z. G. Geng, J. Zhu, C. W. Qiu, X. F. Zhu, Chirality-assisted three-dimensional acoustic Floquet lattices. *Phys. Rev. Res.* **1**, 033149 (2019).
26. A. Darabi, X. Ni, M. Leamy, A. Alù, Reconfigurable Floquet elastodynamic topological insulator based on synthetic angular momentum bias. *Sci. Adv.* **6**, eaba8656 (2020).
27. R. Fleury, D. L. Sounas, C. F. Sieck, M. R. Haberman, A. Alù, Sound isolation and giant linear nonreciprocity in a compact acoustic circulator. *Science* **343**, 516–519 (2014).
28. Y. Ding, Y. Peng, Y. Zhu, X. Fan, J. Yang, B. Liang, X. Zhu, X. Wan, J. Cheng, Experimental demonstration of acoustic chern insulators. *Phys. Rev. Lett.* **122**, 014302 (2019).
29. Y. Wang, B. Yousefzadeh, H. Chen, H. Nassar, G. Huang, C. Daraio, Observation of nonreciprocal wave propagation in a dynamic phononic lattice. *Phys. Rev. Lett.* **121**, 194301 (2018).
30. C. Qin, Y. Peng, Y. Li, X. Zhu, B. Wang, C. W. Qiu, P. Lu, Spectrum manipulation for sound with effective gauge fields in cascading temporally modulated waveguides. *Phys. Rev. Appl.* **11**, 064012 (2019).
31. Y.-F. Wang, Y.-Z. Wang, B. Wu, W. Chen, Y.-S. Wang, Tunable and active phononic crystals and metamaterials. *Appl. Mech. Rev.* **72**, 040801 (2020).
32. Q. Wang, Y. Yang, X. Ni, Y. L. Xu, X. C. Sun, Z. G. Chen, L. Feng, X. P. Liu, M. H. Lu, Y. F. Chen, Acoustic asymmetric transmission based on time-dependent dynamical scattering. *Sci. Rep.* **5**, 10880 (2015).
33. C. Shen, X. Zhu, J. Li, S. A. Cummer, Nonreciprocal acoustic transmission in space-time modulated coupled resonators. *Phys. Rev. B* **100**, 054302 (2019).
34. Y. Hadad, D. L. Sounas, A. Alu, Space-time gradient metasurfaces. *Phys. Rev. B* **92**, 100304 (2015).
35. Y. Shi, S. Fan, Dynamic non-reciprocal meta-surfaces with arbitrary phase reconfigurability based on photonic transition in meta-atoms. *Appl. Phys. Lett.* **108**, 021110 (2016).
36. C. Qin, F. Zhou, Y. Peng, D. Sounas, X. Zhu, B. Wang, J. Dong, X. Zhang, A. Alù, P. Lu, Spectrum control through discrete frequency diffraction in the presence of photonic gauge potentials. *Phys. Rev. Lett.* **120**, 133901 (2018).
37. L. Zhang, X. Q. Chen, S. Liu, Q. Zhang, J. Zhao, J. Y. Dai, G. D. Bai, X. Wan, Q. Cheng, G. Castaldi, V. Galdi, T. J. Cui, Space-time-coding digital metasurfaces. *Nat. Commun.* **9**, 4334 (2018).
38. A. M. Shaltout, V. M. Shalaev, M. L. Brongersma, Spatiotemporal light control with active metasurfaces. *Science* **364**, eaat3100 (2019).
39. J. W. Zang, D. Correas-Serrano, J. T. S. Do, X. Liu, A. Alvarez-Melcon, J. S. Gomez-Diaz, Nonreciprocal wavefront engineering with time-modulated gradient metasurfaces. *Phys. Rev. Appl.* **11**, 054054 (2019).
40. X. Guo, Y. Ding, Y. Duan, X. Ni, Nonreciprocal metasurface with space-time phase modulation. *Light Sci. Appl.* **8**, 123 (2019).
41. H. Lissek, R. Boulandet, R. Fleury, Electroacoustic absorbers: Bridging the gap between shunt loudspeakers and active sound absorption. *J. Acoust. Soc. Am.* **129**, 2968–2978 (2011).
42. W. Klippel, Dynamic measurement and interpretation of the nonlinear parameters of electrodynamic loudspeakers. *J. Audio Eng. Soc.* **38**, 944–955 (1990).
43. B. H. Song, J. S. Bolton, A transfer-matrix approach for estimating the characteristic impedance and wave numbers of limp and rigid porous materials. *J. Acoust. Soc. Am.* **107**, 1131–1152 (2000).
44. E. Galiffi, Y. T. Wang, Z. Lim, J. B. Pendry, A. Alù, P. A. Huidobro, Wood anomalies and surface-wave excitation with a time grating. *Phys. Rev. Lett.* **125**, 127403 (2020).
45. Y. Li, X. Jiang, B. Liang, J.-c. Cheng, L. Zhang, Metascreen-based acoustic passive phased array. *Phys. Rev. Appl.* **4**, 024003 (2015).

46. L. Quan, D. L. Sounas, A. Alù, Nonreciprocal willis coupling in zero-index moving media. *Phys. Rev. Lett.* **123**, 064301 (2019).
47. F. Zangeneh-Nejad, R. Fleury, Doppler-based acoustic gyrator. *Appl. Sci.* **8**, 1083 (2018).
48. F. Zangeneh-Nejad, R. Fleury, Acoustic rat-race coupler and its applications in non-reciprocal systems. *J. Acoust. Soc. Am.* **146**, 843–849 (2019).

Acknowledgments: Z.C. acknowledges discussions with T. Xu and R. Wu and thanks Y. Hui, Y. Jiang, W. Wang, and Z. Wang for the experimental help. **Funding:** This work was supported by the National Key R&D Program of China (grant no. 2017YFA0303700), the National Natural Science Foundation of China (grant nos. 11634006, 11674119, 11690030, 11690032, 11374157, and 81127901), the National Science Foundation EFRI program (grant no. 1641069), the Air Force Office of Scientific Research MURI program (grant no. FA9550-18-1-0379), the Simons Foundation and a Vannevar Bush Faculty Fellowship, the Innovation Special Zone of National Defense Science and Technology, High-Performance Computing Center of Collaborative Innovation Center of Advanced Microstructures, and a project funded by the Priority Academic Program Development of Jiangsu Higher Education Institutions. **Author contributions:** Z.C., Y.P., and A.A. conceived the idea and designed the experiment. Z.C., H.L., J.L., and Y.D. prepared the samples and performed the experiment. Z.C. conducted numerical simulations. Z.C., Y.P., X.-F.Z., B.L., and A.A. contributed to the writing of the paper. X.-F.Z., B.L., Y.L., A.A., and J.C. supervised the entire study. **Competing interests:** The authors declare that they have no competing interests. **Data and materials availability:** All data needed to evaluate the conclusions in the paper are present in the paper and/or the Supplementary Materials.

Submitted 21 April 2021
Accepted 15 September 2021
Published 3 November 2021
10.1126/sciadv.abj1198

ScienceAdvances

Efficient nonreciprocal mode transitions in spatiotemporally modulated acoustic metamaterials

Zhaoxian ChenYugui PengHaoxiang LiJingjing LiuYujiang DingBin LiangXue-Feng ZhuYanqing LuJianchun ChengAndrea Alù

Sci. Adv., 7 (45), eabj1198.

Science Advances (ISSN) is published by the American Association for the Advancement of Science. 1200 New York Avenue NW, Washington, DC 20005. The title *Science Advances* is a registered trademark of AAAS.